Desalination and Water Treatment
www.deswater.com

doi: 10.5004/dwt.2022.28332

254 (2022) 274–286
April

Preparation of cobalt ferrite nanoparticles and application as peroxymonosulfate activators for the removal of Congo red

Zulhumar Musajan, Pengfei Xiao*, Jing Zhao, Shuang Han, Qirui Wang

College of Forestry, Northeast Forestry University, Harbin 150040, China, emails: xpfawd@nefu.edu.cn (P. Xiao)
ORCID: 0000-0002-0379-4358; 1344663598@qq.com (Z. Musajan), 2168952162@qq.com (J. Zhao), 2323643177@qq.com (S. Han), 846951244@qq.com (Q. Wang)

Received 6 November 2021; Accepted 16 February 2022

ABSTRACT

Persulfate-based advanced oxidation processes have been widely considered efficient remediation methods, and ferrite is a satisfactory activator of persulfate (PS) for the removal of environmental pollutants. Herein, cobalt ferrite nanoparticles (nano-$CoFe_2O_4$) were synthesized by the co-precipitation method and used to activate peroxymonosulfate (PMS) for the degradation of Congo red (CR) in aqueous solution. The results of characterization analysis showed that these nanoparticles exhibit an average crystallite size in the range of 13.96–25.17 nm, with a spherical structure, rich functional groups on their surfaces, and excellent magnetic and thermal stability. Furthermore, degradation experiments were designed to investigate the effects of a single factor, including the initial CR concentration, PMS concentration, catalyst dosage, initial pH and coexisting ions. The corresponding removal behaviour is in good agreement with the pseudo-first-order dynamics model. In addition, in the nano-$CoFe_2O_4$/PMS system, according to the identification results of reactive oxygen species, superoxide radical ($^{\bullet}O_2^-$) and singlet oxygen radical ($^1O_2$) species were the major active species that degraded CR, and the mechanism of PMS activation was comprehensively proposed. Meanwhile, after nano-$CoFe_2O_4$ was used five times continuously, the CR removal efficiency in the nano-$CoFe_2O_4$/PMS system decreased by only 7%, indicating that the prepared catalyst has excellent reusability. Therefore, the nano-$CoFe_2O_4$ synthesized in this research represents a novel, economical and efficient activator of PMS for the degradation of organic dyes in industrial wastewater.

Keywords: Cobalt ferrite nanoparticles; Congo red; Persulfate-based advanced oxidation; Heterogeneous catalyst; Reaction mechanism

1. Introduction

In recent years, organic dyes have been incorporated into several industries, including textile, printing and dyeing, papermaking, rubber, plastic, and food industries and other processing industries [1–3]. Moreover, most organic dyes with complex structural components cannot be easily removed from water, which also causes carcinogenicity, sensitization and reproductive toxicity to the human body [4,5]. Congo red (CR) is an organic dye with a complex aromatic structure and a typical azo dye that has two unsaturated chromogenic groups (azo groups) and four colour-assisting groups (amino groups and sodium sulfonate groups), showing high thermal stability and reasonable physical and chemical stability [6,7]. CR is widely used to colour cotton fibres and to serve as an acid-base indicator in other industries, but it has a high loss rate during manufacturing and use [8,9]. The discharge of CR wastewater into natural water not only leads to serious deterioration of water quality and prevents the growth of aquatic organisms and microorganisms but also poses a serious threat to human health, such as dysfunction, carcinogenesis and

* Corresponding author.

harm to unborn babies [10,11]. Therefore, developing new and efficient processing methods is crucial for the removal of azo dye pollutants from aqueous solutions.

At present, the effective removal methods of azo dyes mainly include biodegradation [12,13], adsorption [14,15], photocatalysis [16,17] and flocculation [18]. In addition to these traditional technologies, there has been a recent explosion in advanced oxidation technology with fast speed, high efficiency and strong oxidation capacity for removing dyes [19,20]. Meanwhile, persulfate-based advanced oxidation processes have been gaining much attention over recent years, possessing the advantages of strong reaction stability, mild reaction conditions and environmental friendliness [21]. In this system, the sulfate radical ($SO_4^{-\bullet}$, E_0 = 2.5~3.1 V), which is generated during persulfate (PS) activation, possesses the ability to degrade strongly bonded organic contaminants to simple harmless molecules better than PS itself [22]. There are many methods used to activate PS, such as thermal activation, ultrasonic activation, ultraviolet activation, microwave activation, alkali activation, and transition metal activation [23]. The key limitation of the external energy activation methods not only requires relatively massive energy but also harsh reaction conditions [24]. Readily available metal materials that hardly require additional energy have attracted increasing attention.

In the process of using metal materials to activate PS, the surface of the catalyst plays an important role in the catalytic process because the reaction is often carried out on the surface of the catalyst [25,26]. Consequently, metal nanoparticles with special mechanical, magnetic and optical properties have been gaining importance in persulfate-based advanced oxidation systems due to their small particle size, large specific surface area and high specific surface energy [27]. Among them, cobalt ferrite nanoparticles (nano-$CoFe_2O_4$) have astonishing stability, magnetism, recyclability and synergistic effects between Co and Fe, making them a good choice as PS activators [28]. Additionally, nano-$CoFe_2O_4$ greatly reduces the leaching rate of heavy metals from the solid phase due to its unique and stable spinel structure [29]. Nevertheless, in previous research, nano-$CoFe_2O_4$ as a catalyst for peroxymonosulfate (PMS) has not been reported for dye degradation.

In this research, nano-$CoFe_2O_4$ was synthesized by a co-precipitation method and used to activate peroxymonosulfate (PMS) for the degradation of CR. The main purpose of the article is to (1) characterize the synthesized nano-$CoFe_2O_4$ by a comprehensive characterization method and analyse the physical characteristics of the synthesized catalyst; (2) analyse and discuss the effect of different influencing factors on the degradation efficiency of CR and carry out pseudo-first-order kinetics studies; (3) clarify the possible mechanism of PMS activation by nano-$CoFe_2O_4$; and (4) research the stability and reusability of nano-$CoFe_2O_4$.

2. Experimental

2.1. Chemicals and reagents

Congo red ($C_{32}H_{22}N_6Na_2O_6S_2$), iron nitrate hydrate ($FeN_3O_9{\cdot}9H_2O$), cobalt nitrate hexahydrate ($Co(NO_3)_2{\cdot}6H_2O$, 99.99% metal basis), potassium monopersulfate triple salt ($KHSO_5{\cdot}0.5KHSO_4{\cdot}0.5K_2SO_4$, ≥42% $KHSO_5$ basis), sodium hydroxide (NaOH, 96%), ethanol (EtOH, AR, ≥99.5%), tert-butanol (TBA, GR, ≥99.5%), furfuryl alcohol (FFA, CP, 97%), p-benzoquinone (p-BQ, 99%), methanol (MT, AR, 99.5%), sodium chloride (NaCl, 99.5%), sodium bicarbonate ($NaHCO_3$, 99.5%), sodium carbonate (Na_2CO_3, 99.8%), potassium nitrate (KNO_3, >99%), and potassium dihydrogen phosphate (KH_2PO_4, 99.5%) were purchased from Aladdin Industrial Corporation (Shanghai, China). In the experimental process, all the reagents were analytically pure, and all solutions were prepared with ultrapure water.

2.2. Synthesis of nano-$CoFe_2O_4$

In related references, the reaction process of preparing the catalyst by the coprecipitation method is relatively stable, and the obtained catalyst is relatively pure [30]. Consequently, nano-$CoFe_2O_4$ was fabricated by the coprecipitation method as follows: $Co(NO_3)_2{\cdot}H_2O$ (0.01 mol) and $Fe(NO_3)_3{\cdot}9H_2O$ (0.02 mol) were dissolved in 100 mL of ultrapure water and ultrasonically (80 W) dispersed for 10 min to achieve uniform dispersion in the solution. Then, the solution was stirred continuously in a heated water bath (60°C) for 0.5 h. NaOH solution (4 mol) was added gradually to the mixed solution so that the pH value rose to approximately 11–13 and complete precipitation occurred, and the solution was stirred for 2 h in a heated water bath (80°C). Afterwards, the red–brown solid was washed with ultrapure water several times until a neutral pH value was reached. Finally, the red–brown solid was dried at 70°C for 10 h and poured into a crucible for roasting in a muffle furnace (SX-G02103, Tianjin, China). The temperature inside the muffle furnace was raised to 500°C and maintained at this temperature for 2 h. Nano-$CoFe_2O_4$ was obtained and fully ground for experimental application.

2.3. Activation of PMS by nano-$CoFe_2O_4$ for CR degradation

The catalytic activity of nano-$CoFe_2O_4$ for activating PMS was investigated by CR degradation experiments. In all batches of experiments, the CR degradation experiments were conducted in a series of 250 mL conical flasks. Fifty millilitres of each of the prepared CR solution and PMS solution was poured into the flasks, and the catalyst (nano-$CoFe_2O_4$) was rapidly added to the reactors. Then, the conical flasks were placed in a thermostatic air bath shaker at 25°C and 160 rpm to initiate the reaction. Except for the variable factor, the nano-$CoFe_2O_4$ dose and the initial concentrations of PMS and CR were 0.5 g/L, 0.5 mmol/L, and 0.2 g/L, respectively. The initial pH of the solution was not consciously adjusted, with an approximate value of 6. To evaluate the adsorption effect of nano-$CoFe_2O_4$ on CR, adsorption experiments were performed, and the nano-$CoFe_2O_4$ dose and initial concentration of CR were 0.5 and 0.2 g/L, respectively. After the treatment, 3 mL of sample supernatant was filtered through a 0.45 μm filter into a cuvette every 5 or 10 min, and the supernatant was immediately analysed to determine the residual CR concentration using a UV-1800 instrument at 497 nm.

For the reusability experiments, the catalysts used after the previous reaction cycle were collected with a magnet,

thoroughly rinsed with ultrapure water to remove remnants, dried at 80°C for 5 h, and recovered four times continuously by following the above process. Single-variable control trials were carried out to research and optimize the removal conditions, including initial pH (3.0–11.0), initial CR concentration (0.05–0.3 g/L), PMS concentration (0.1–0.5 mmol/L), $CoFe_2O_4$ dose (0.1–0.5 g/L) and reaction time (0–60 min). In all degradation experiments, experimental data were obtained by calculating the average of the results of three parallel experiments.

2.4. Analytical methods

To analyse the surface topography, diffraction peaks, elemental composition, functional groups, magnetic properties and thermal stability, catalysts were detected by characterization methods, including scanning electron microscopy (SEM, SU8020, Hitachi, Japan), X-ray powder diffraction (XRD, Tongda, China), X-ray photoelectron spectrometer spectroscopy (XPS, Thermo Escalab 250 Xi, US), Fourier-transform infrared (FT-IR) spectroscopy (Nicole-iS 10 FT-IR spectrometer, US), vibrating-sample magnetometry (VSM, Quantum Design, US) and thermogravimetric analysis (TGA, Netzsch, Germany). Furthermore, the concentration of CR was determined with a maximum wavelength of 497 nm using a ultraviolet–visible (UV–Vis) spectrophotometer (UV-1800, Mapada, China). Electron paramagnetic resonance (EPR) spectra were obtained by an electron paramagnetic resonance device (A300-10/12, Bruker, Germany) to identify the radicals generated from the nano-$CoFe_2O_4$/PMS system. The UV–Vis absorption spectra were documented with a UV–Vis spectrophotometer (TU-1901, PERSEE, China). The total organic carbon (TOC) was measured using a TOC-L CPN analyser (TD-3500, Dandong, China). In the nano-$CoFe_2O_4$/PMS system, pseudo-first-order kinetics were used to fit the kinetics characteristics of the removal of CR [Eq. (1)], and the K_{app} value was obtained. The removal rate of CR is calculated by Eq. (2) as follows:

$$-\ln\left(\frac{C}{C_0}\right) = kt \tag{1}$$

$$\eta = \frac{\left(C_0 - C\right)}{C_0} \tag{2}$$

where C_0 (mg/L) and C (mg/L) are the initial CR concentration and CR concentration at time t (min), respectively.

3. Results and discussion

3.1. Characterization of nano-$CoFe_2O_4$

The changes in the morphological characteristics of the prepared catalysts were analysed by SEM before and after the degradation reaction. It is clear from Fig. 1a that nano-$CoFe_2O_4$ consists of uniformly distributed spherical particles. Additionally, seen from the high-magnification SEM images, shown in Fig. 1b, the average diameter of nano-$CoFe_2O_4$ is in the range of 13–25 nm, which is obtained by nano measurer. The prepared spherical nano-$CoFe_2O_4$

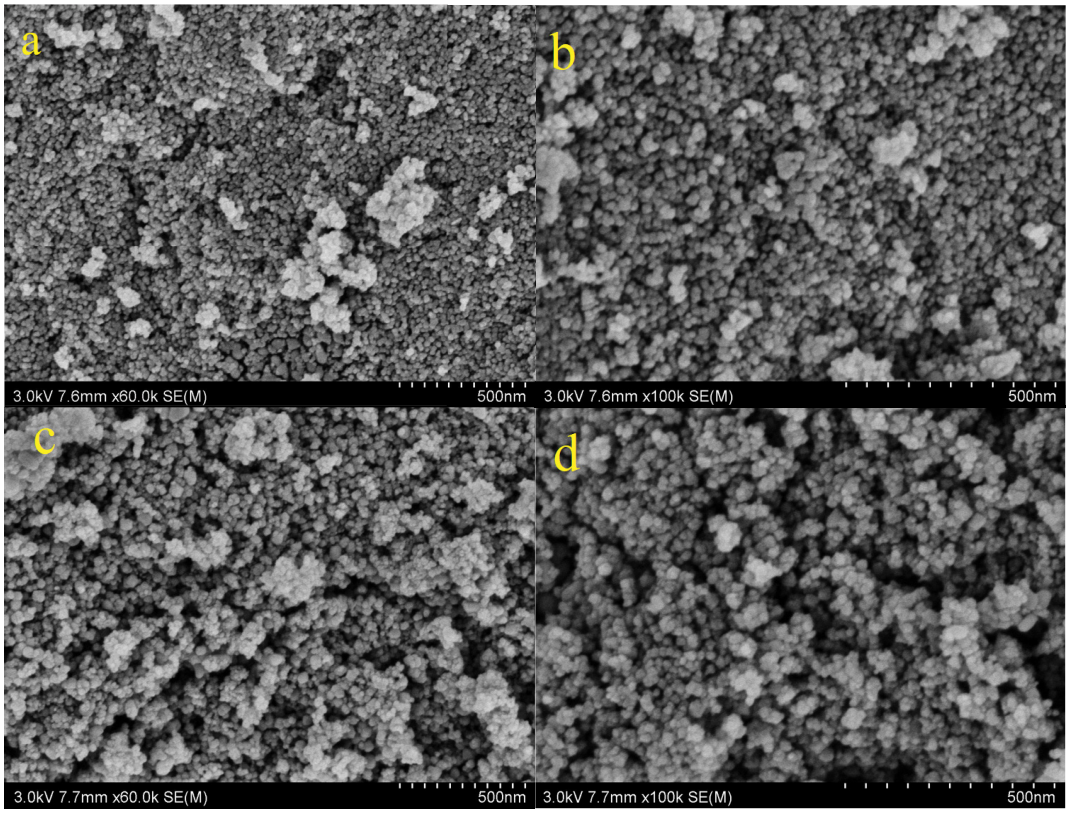

Fig. 1. SEM images of nano-$CoFe_2O_4$ before (a, b) and after (c, d) reaction.

possesses small particles with enlarged surface areas and a substantial number of reaction sites, which is beneficial to CR degradation, as the contact area between CR and nano-$CoFe_2O_4$ is increased. Moreover, Fig. 1c and d show that some of the nanoparticles gathered together after the reaction, which confirmed that nano-$CoFe_2O_4$ had defects in aggregation after participating in the reaction [31].

XPS measurements were carried out in a Thermo Escalab 250 Xi spectrometer, equipped with a charge neutralizer and monochromatic Al kα (1486.6 eV) radiation source spectrometer. Fig. 2a illustrates the XPS spectrum of nano-$CoFe_2O_4$, in which the binding energy of each element was corrected by a C1 peak at 284.8 eV to analyse the chemical status and chemical composition. The sample contains Co, Fe, and O, with binding energies at 780.0, 710.7 and 529.7 eV, respectively, accounting for 12.95%, 25.34%, and 46.99%; this outcome is consistent with Kirankumar and Sumathi's research conclusion [32]. As shown in Fig. 2b, the peak at 795.5 eV conformed well to Co^{3+}. The peaks at 780.0 and 782.5 eV are attributed to Co^{2+} in octahedral sites and tetrahedral sites, respectively. Moreover, the peaks at 786.7 and 802.8 eV are related to the shakeup excitation of high-spin Co^{2+}. The Fe2p spectra consist of $Fe2p_{1/2}$ and $Fe2p_{3/2}$ peaks, and the peak at 724.2 eV corresponds to $Fe2p_{1/2}$ from Fig. 2c. The $Fe2p_{3/2}$ spectra were asymmetric and divided into two peaks with binding energies of 710.7 and 713.4 eV. Fig. 2d shows that the O1s spectra exhibits two peaks at 529.7 and 531.1 eV, which are consistent with the surface hydroxyl species. All the XPS analysis results further indicate the formation of nano-$CoFe_2O_4$ [33].

Crystallinity and phase analysis was performed by XRD using Cu kα radiation (λ = 0.15406 nm) over 2θ = 5°–70°. As shown in Fig. 3a, the XRD analysis confirms the crystallinity and phase purity of spinel nano-$CoFe_2O_4$ before and after reaction. The diffraction peaks observed for nano-$CoFe_2O_4$ at 2θ = 30.54°, 35.66°, 43.02°, 57.26°, 62.62° completely matched the (220), (311), (400), (511) and (440) reflections, respectively, which is basically consistent with the results of Naik's and Wu's research [34,35]. Moreover, by comparing the peak intensity changes before and after the reaction, the X-ray diffraction pattern does not change significantly, which indicates that the catalyst material has outstanding reaction stability in phase composition and crystal structure. Furthermore, according to Scherrer's equation [Eq. (3)], the average size of each nano-$CoFe_2O_4$ was in the range of 15–44 nm, which was consistent with the SEM analysis results.

$$D = \frac{K\lambda}{B\cos\theta} \tag{3}$$

where D represents the crystallite size (nm), K = 0.89 (Scherrer constant), λ = 0.15406 (the X-ray wavelength), B represents

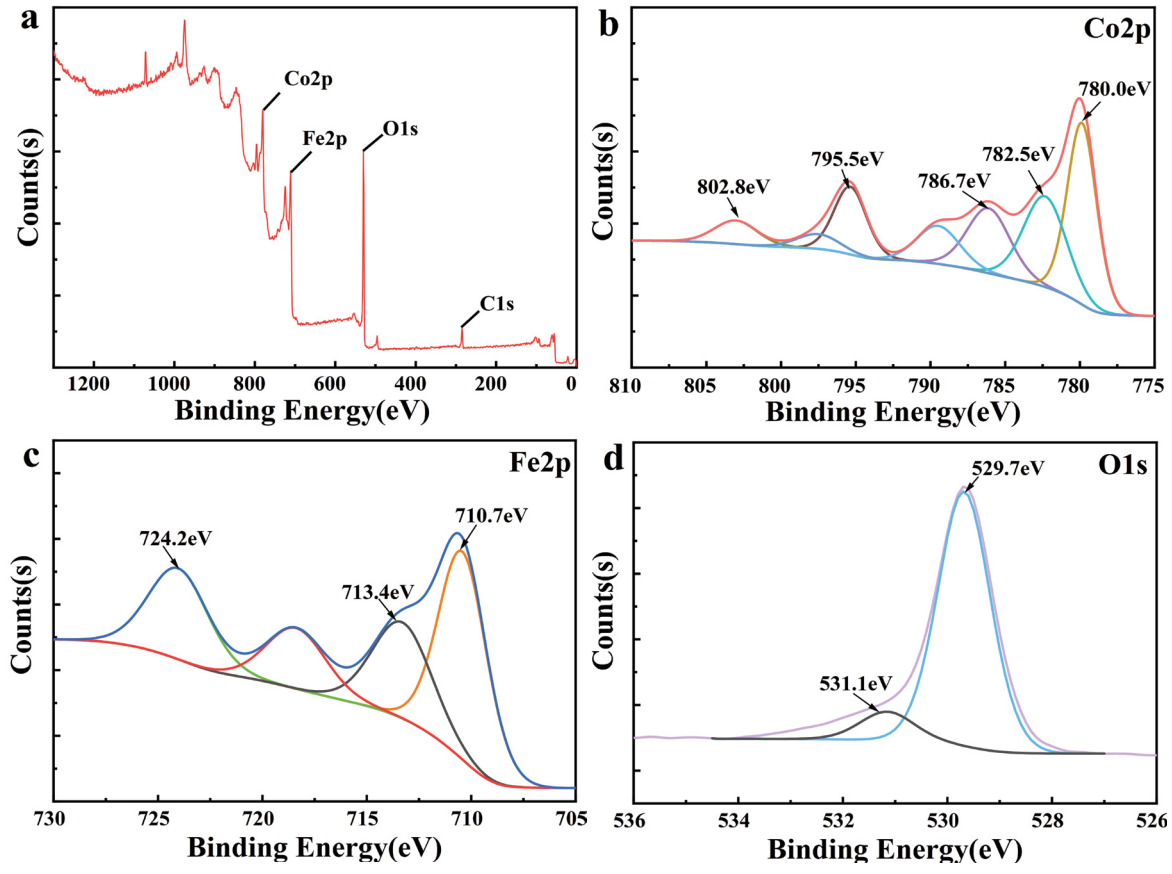

Fig. 2. XPS survey spectra (a), Co 2p XPS spectra (b), Fe 2p XPS spectra (c) and O1s XPS spectra (d) of nano-$CoFe_2O_4$.

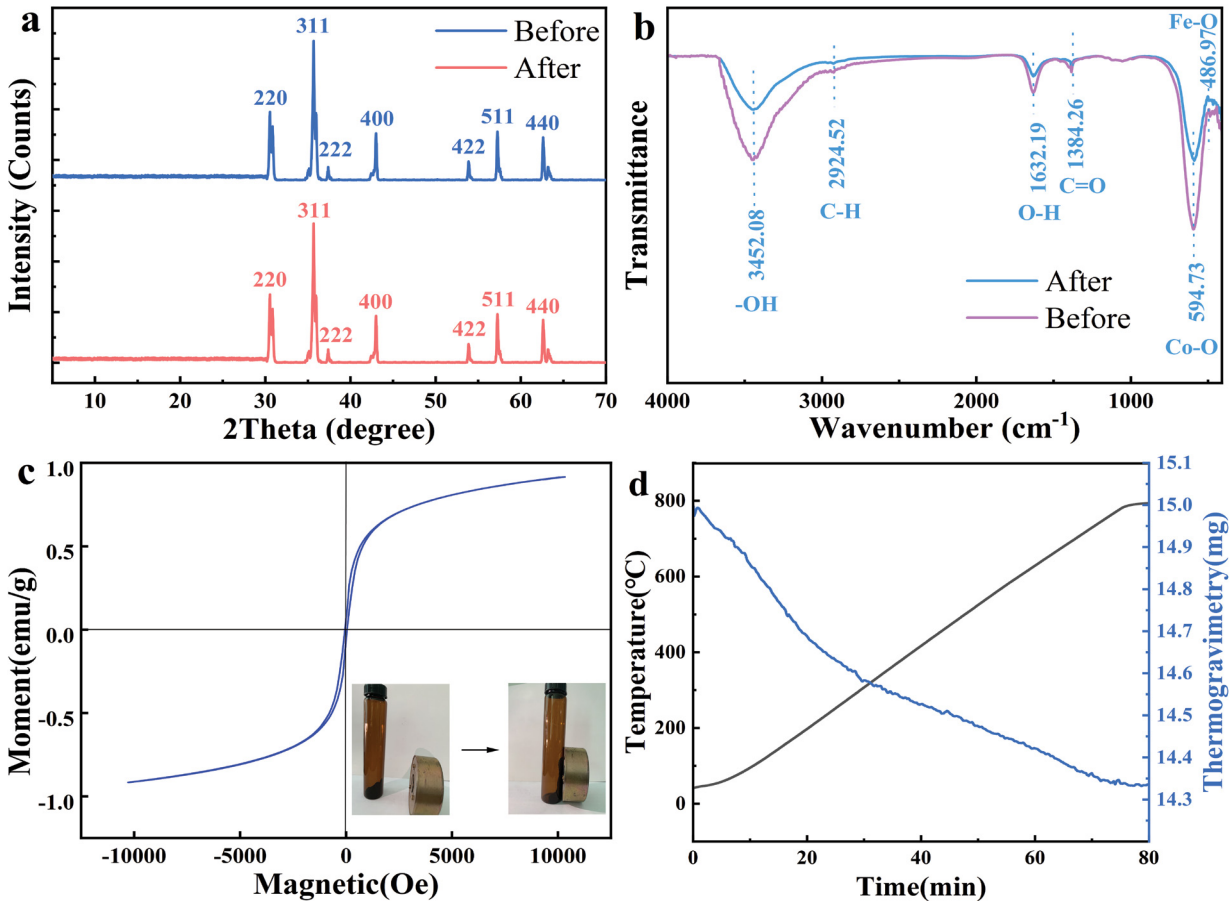

Fig. 3. XRD patterns (a), FT-IR spectra (b), VSM analysis (c) and TGA analysis (d) of nano-$CoFe_2O_4$.

the full width at half maximum of the diffraction peak and θ represents the Bragg diffraction angle.

The FT-IR spectra of nano-$CoFe_2O_4$ before and after the reaction are shown in Fig. 3b. In $CoFe_2O_4$ nanoparticles, the two absorption bands at 486 and 594 cm^{-1} were relevant to the stretched vibrations of the Co–O and Fe–O bonds in the octahedral and tetrahedral sites of the spinel ferrites. The peaks at approximately 3,452; 2,924; 1,632 and 1,384 cm^{-1} were attributed to –OH stretching, O–H stretching, C–H stretching, O–H stretching, and C=O bending [36]. Obviously, nano-$CoFe_2O_4$ is nearly unchanged after reaction, except that the intensity of the two peaks decreases, indicating that the chemical structure of the prepared catalyst is relatively stable.

Previous studies indicate that ferrite nanoparticles possess excellent magnetic properties and have been considered for a wide range of industrial applications for a long time [37]. Consequently, the magnetic properties of nano-$CoFe_2O_4$ were determined using VSM. Fig. 3c presents plots of magnetization vs. the applied external magnetic field at room temperature for nano-$CoFe_2O_4$. The saturation magnetization of nano-$CoFe_2O_4$ under ambient conditions approached 41.54 emu/g, illustrating that nano-$CoFe_2O_4$ exhibited strong magnetic responsiveness. The inset picture in Fig. 3c also proves that nano-$CoFe_2O_4$ can be easily attracted to the vial wall by a permanent magnet.

TGA was used to measure the relationship between the quality of the catalyst and temperature or time under the control of the program temperature and was employed to determine the thermal stability of the catalyst [38]. The samples were heated from 0 to 900°C at a heating rate of 10°C/min for almost 80 min, as shown in Fig. 3d. From the TGA curve, the catalyst lost less than 0.1 g during heating, with its mass decreasing from 15.0 g to approximately 14.34 g, which also demonstrates that the catalyst has excellent thermal stability. The reason for the weight loss and weight loss rate reflects the extent of oxygen loss and the speed of oxygen loss in different temperature regions, respectively, during heating.

3.2. Removal of CR in different systems

Preliminary experiments were conducted in different systems, which have different effects on CR removal, and the results are shown in Fig. 4a. Obviously, when nano-$CoFe_2O_4$ was used alone, the concentration of CR did not decrease significantly and only accounted for about 3.5% in 60 min, demonstrating that the adsorption effect of nano-$CoFe_2O_4$ on CR was very poor. PMS itself plays a role in the removal of CR, but the degradation effect is only approximately 40% in 60 min. However, the removal efficiency of CR was up to 90% in the $CoFe_2O_4$/PMS system, indicating

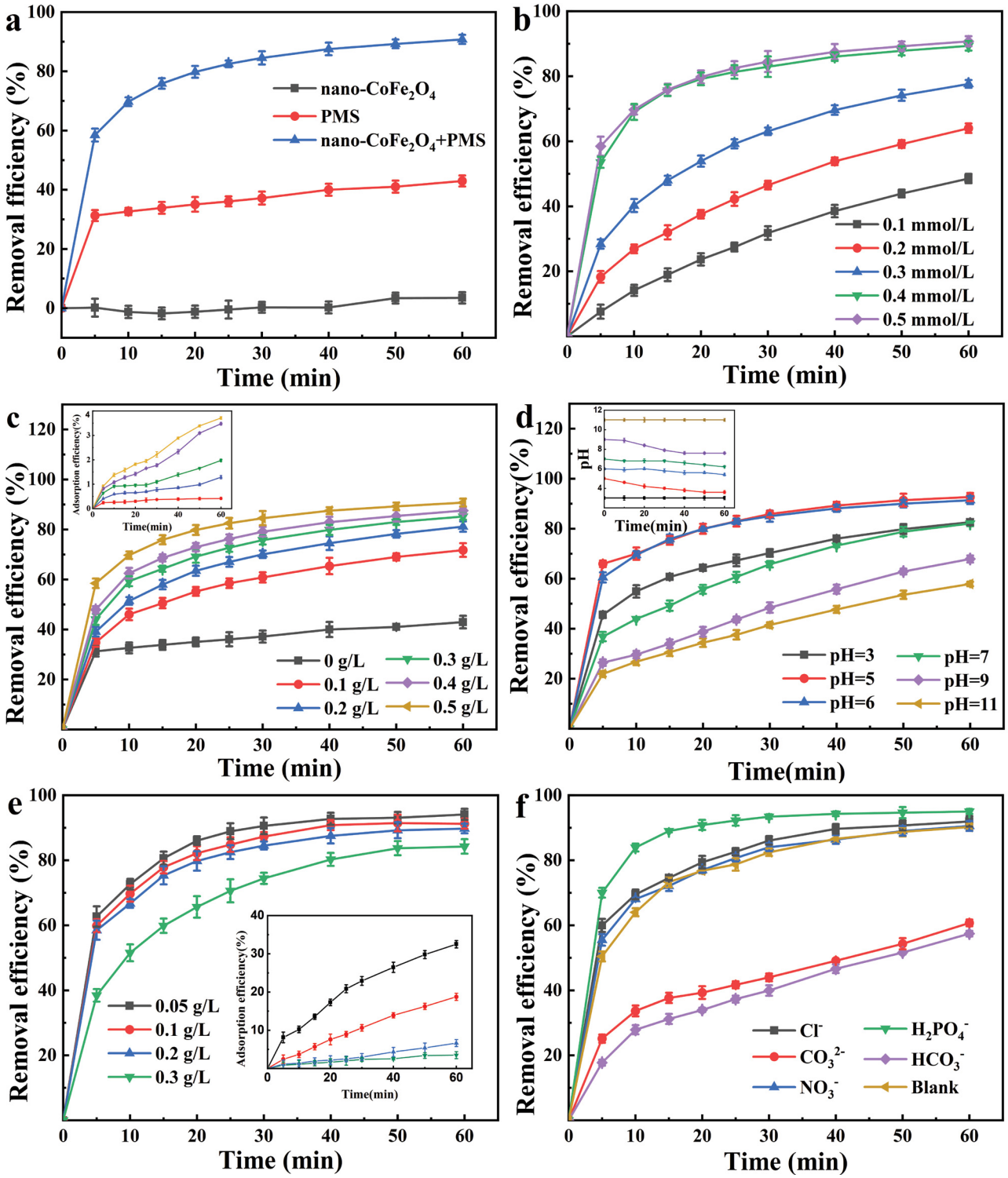

Fig. 4. Degradation of CR in different systems (a), effect of PMS concentration (b), effect of nano-$CoFe_2O_4$ dose (c), effect of initial pH (d), effect of initial CR concentration (e) and effect of coexisting ions (f).

that the catalyst has the ability to activate PMS, and PMS produces active species to degrade CR rapidly. This result also showed that CR removal in the $CoFe_2O_4$/PMS system occurs by oxidative degradation rather than adsorption. Under the optimal conditions, a key preponderance of this research is that the CR degradation efficiency by activating PMS with nano-$CoFe_2O_4$ is substantially higher than that of other studies [39].

3.3. Experimental condition optimization

3.3.1. Effect of PMS concentration

The effect of PMS concentration on CR degradation efficiency in the nano-$CoFe_2O_4$/PMS system is summarized in Fig. 4b. After 5 min, the degradation rate of CR by 0.5 mmol/L PMS significantly increased to 58.47%, which was nearly 8 times higher than the degradation rate of the 0.1 mmol/L PMS system. When the PMS concentrations were 0.1, 0.2, 0.3, 0.4 and 0.5 mmol/L, the K_{app} values of CR degradation were 0.0110, 0.0159, 0.0231, 0.0309 and 0.0329 min^{-1}, respectively, showing an increasing trend. This may be explained by the production of more reactive oxygen species (ROS) in the activation system and an increase in the contact frequency between CR molecules and ROS. This phenomenon has also been observed in previous studies, where an increase in the concentration of PMS provides more ROS and accelerates CR degradation in the activated systems [40]. However, when the PMS concentration was from 0.4 to 0.5 mmol/L, there was no significant increase in CR degradation efficiency, which may be due to the quenching reaction between PMS that activated to produce excess ROS and unconsumed PMS [41]. Oh et al. studied activation of PMS by nano-$CoFe_2O_4$ for the degradation of sulfamethoxazole, which was that the increase of PMS concentration makes the degradation efficiency of pollutants more obvious, but the concentration of PMS (2 mmol/L) used in the experiment is greatly higher than that in this experiment [42].

3.3.2. Effect of nano-$CoFe_2O_4$ dose

As shown in Fig. 4c, the increase in nano-$CoFe_2O_4$ dose was instrumental in improving the CR degradation efficiency, and the degradation rate continuously increased from 71.75% to 90.76%. Meanwhile, the K_{app} value (0.0329 min^{-1}) is highest when the nano-$CoFe_2O_4$ dose is 0.5 g/L, and nearly 2 times higher than the K_{app} value (0.0177 min^{-1}) of the 0.1 g/L nano-$CoFe_2O_4$ dose. These findings are very consistent with previous studies showing that the degradation efficiency of activated PMS continuously increases because an increase in the amount of nano-$CoFe_2O_4$ might provide more activation factors in the activated system to participate in and accelerate CR degradation [43]. Nevertheless, when the amount of catalyst is increased to 0.3 g/L or above, it was not obvious to the degradation efficiency of catalyst on pollutants. This phenomenon can be interpreted as the magnetic aggregation caused by excessive catalyst, which decreased the number of effective active sites and leads to degradation efficiency. Another reason for the low degradation efficiency is that too many free radicals are generated at the same time, which leads to the quenching between free radicals. Shao et al. [44] concluded that $CoFe_2O_4$ for was a PMS activator with excellent stability in their research, and found that increasing the $CoFe_2O_4$ dose could provide more surface area and active sites to promote the activation of PMS and removal of amlodipine. On the other hand, the maximum adsorption rate of CR by nano-$CoFe_2O_4$ is only 3.71%, even if the dose is the highest at 0.5 g/L.

3.3.3. Effect of initial pH

Because of the activation of PMS and the CR degradation related to the pH of aqueous solution, the effect of the initial pH value on the CR degradation efficiency was researched. Fig. 4d shows the degradation of CR in the nano-$CoFe_2O_4$/PMS system at pH = 3, 5, 6 (without pH adjustment), 7, 9, and 11. After the start of the reaction, the CR degradation rates at pH = 5 and 6 are almost the same and are significantly higher than those at other pH values. However, CR degradation under alkaline conditions is slower; for instance, the CR degradation rate at pH = 11 is 40% lower than that at pH = 5 after 5 min. According to the research results of Guan et al., under weak acidic conditions (pH = 5, 7), nano-$CoFe_2O_4$/PMS system showed more significant degradation of sulfosalicylic acid, demonstrating HSO_5^- was the predominant PMS species at weak acidic and neutral conditions [45].

Additionally, during the whole experiment, the pH value hardly changed under alkaline conditions, but there was a slight downwards trend under neutral and acidic conditions. Although this phenomenon indicated that the pH conditions for PMS activation by nano-$CoFe_2O_4$ are more extensive, the reaction of degrading CR by activating PMS is more suitable to be carried out under weakly acidic conditions rather than strong alkaline conditions. This is because under strong alkali conditions, activation generates $SO_4^{-\bullet}$, the surrounding hydroxyl ions (OH^-) react to form hydroxyl radicals ($^\bullet OH$), and the $^\bullet OH$ species are quickly converted into oxygen free radicals ($O^{-\bullet}$). Because the activity of $O^{-\bullet}$ is much weaker than that of $SO_4^{-\bullet}$, CR degradation slows down, which is consistent with the results of previous studies [46]. The reaction formulas are as follows in Eqs. (4) and (5):

$$SO_4^{-\bullet} + OH^- \rightarrow SO_4^{2-} + {}^\bullet OH \quad (4)$$

$${}^\bullet OH + H_2O \rightarrow O^{-\bullet} + HO_3^+ \quad (5)$$

3.3.4. Effect of initial CR concentration

The effect of different initial concentrations of CR on the degradation effect is shown in Fig. 4e. When the initial CR concentration was 0.05 g/L, the degradation rate reached 86.04% after 20 min, which was 20.39% higher than the initial CR concentration of 0.3 g/L. Therefore, as the initial CR concentration increases, the degradation rate gradually decreases. The decrease in the CR degradation rate can be explained by CR molecules competing for a limited number of active substances. The PMS concentration is fixed when the CR concentration increases in the experiment. However, after 1 h of reaction, the difference between the degradation rates of different systems decreased, and the degradation rate was in the range of 84% to 95%. In addition, the adsorption rate decreased from 32.5% to 3.48% after 60 min, with the initial concentration increasing from 0.05 to 0.3 g/L. The above results indicated that the nano-$CoFe_2O_4$/PMS system is suitable for a wide concentration range of CR and could show a good removal effect, which was quite considerable compared with the results of previous research [47].

3.3.5. Effect of coexisting ions

Practical application tests are needed, because there are many anions in wastewater or natural water that can affect PMS activation or the removal of contaminants [48]. The degradation efficiency of CR in the nano-$CoFe_2O_4$/PMS system in the presence of 50 mmol/L inorganic anions such as Cl^-, CO_3^{2-}, HCO_3^-, $H_2PO_4^-$ and NO_3^- can be found in Fig. 4f. Obviously, after adding CO_3^{2-} and HCO_3^-, the CR degradation efficiency decreased, and the CR degradation rate was inhibited by 30% and 37% within 10 min, respectively. This is mainly because CO_3^{2-} and HCO_3^- are scavengers of hydroxyl and sulfate radicals [Eqs. (6) and (7)] [49]. However, after a 10 min reaction, the difference between the degradation rates of the system with the addition of two ions and the control gradually narrowed to within 10%. The results also indicated that the CR degradation rates were virtually unchanged with the addition of NO_3^-. In contrast, $H_2PO_4^-$ and Cl^- have a promoting effect on the CR degradation rate; in particular, $H_2PO_4^-$ increases the CR degradation efficiency by approximately 20% in 10 min. Previous studies have confirmed that Cl^- will generate multiple active chlorine species including $Cl^•$, $Cl_2^{-•}$, $HOCl^{-•}$ and Cl_2 in the persulfate system, which can promote the degradation of pollutants [Eqs. (8)–(12)] [50]. Furthermore, $H_2PO_4^-$ ionizes H^+ [Eq. (13)] to provide a weakly acidic environment, which is more conducive to the reaction conditions [51]. The study of Jaafarzadeh et al. [52] found that compared with other anions, $H_2PO_4^-$ had more negative effects, $H_2PO_4^-$ had the ability to combine in the catalyst surface, so the $H_2PO_4^-$ greatly decreased the PMS heterogeneous activation.

$$HCO_3^- + SO_4^{-•} \rightarrow H^+ + CO_3^{-•} + SO_4^{2-} \quad (6)$$

$$HCO_3^- + {}^•OH \rightarrow CO_3^{-•} + H_2O \quad (7)$$

$$Cl^- + SO_4^{-•} \rightarrow Cl^• + SO_4^{2-} \quad (8)$$

$$Cl^• + Cl^- \rightarrow Cl_2^{-•} \quad (9)$$

$$Cl^• + OH^- \rightarrow {}^•OH + Cl^- \quad (10)$$

$$Cl_2^{-•} + OH^- \rightarrow HOCl^{-•} + Cl^- \quad (11)$$

$$Cl_2^{-•} + Cl_2^{-•} \rightarrow Cl_2 + 2Cl^- \quad (12)$$

$$H_2PO_4^- \leftrightarrows H^+ + HPO_4^{2-} \quad (13)$$

3.4. Reaction mechanisms

3.4.1. Identification of the ROS

Nanometals generate ROS such as $SO_4^{-•}$, hydroxyl radicals ($^•OH$), superoxide radicals ($^•O_2^-$) and singlet oxygen ($^1O_2$) in the process of activating PMS [53]. The types of reactive oxygen species produced by activation systems may likewise differ for different pollutants [54]. Therefore, it is necessary to use a variety of quenching agents to identify the dominant ROS in the degradation of CR in the nano-$CoFe_2O_4$/PMS system. EtOH and MT were used to quench $SO_4^{-•}$ (K = 1.6–7.8 × 10^7 M/S and K = 0.9–1.3 × 10^7 M/S) and $^•OH$ (K = 1.2–2.8 × 10^9 M/S and K = 0.8–1.0 × 10^7 M/S). TBA, BQ and FFA were used to quench $^•OH$ (K = 3.8–7.6 × 10^8 M/S), $^•O_2^-$ (K = 0.9–1 × 10^9 M/S) and $^1O_2$ (K = 1.2 × 10^8 M/S), respectively. Under the same conditions, the lower degradation rate proved that the more obvious the inhibitory effect is, the greater the influence of ROS on the degradation reaction [55]. To correctly compare the quenching effect, all quenchers employed a concentration of 50 mmol/L.

As shown in Fig. 5a, the degradation rate of CR in the blank control group reached 90.24% in 60 min. After the addition of FFA, the CR degradation efficiency was significantly inhibited and decreased by approximately 31.47%, indicating that the generated $^1O_2$ played a vital role in the nano-$CoFe_2O_4$/PMS reaction system. In addition, BQ suppressed CR degradation, decreasing the degradation

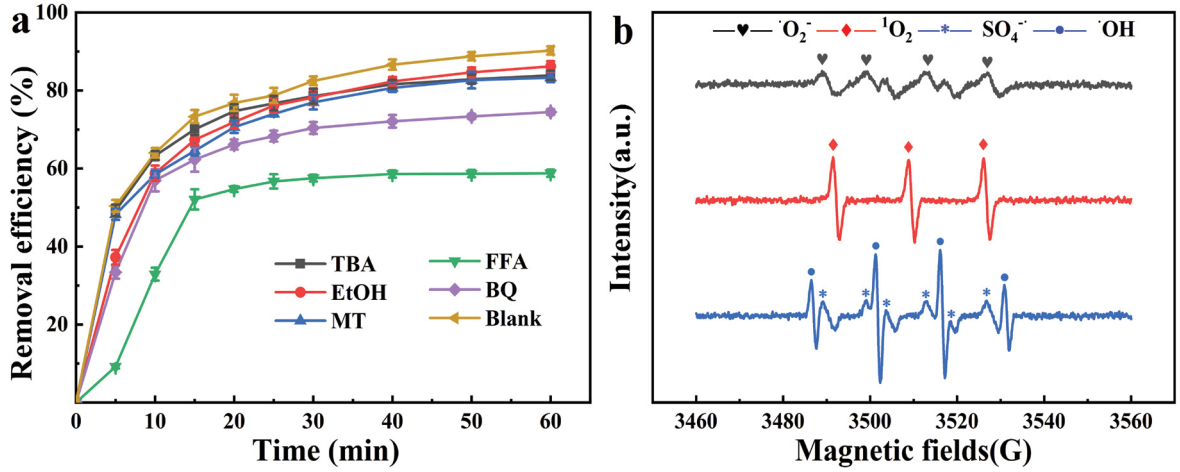

Fig. 5. Effect of free radical scavengers on CR removal efficiency (a) EPR spectra of $^•O_2^-$, $^1O_2$, $SO_4^{-•}$ and $^•OH$ (b).

efficiency by approximately 15.76%, which demonstrated that the produced $^{\bullet}O_2^-$ was also one of the main ROS in the nano-$CoFe_2O_4$/PMS reaction system. However, the addition of TBA, EtOH and MT had a weak inhibition effect on CR degradation efficiency, which revealed that $SO_4^{-\bullet}$ and $^{\bullet}OH$ contribute little to the CR degradation in the nano-$CoFe_2O_4$/PMS system. In conclusion, the results of radical trapping experiments showed that a variety of ROS exist in the reaction system, among which $^1O_2$ and $^{\bullet}O_2^-$ play a major role in the degradation process. The study of Song et al. [56] obtained the results that $SO_4^{-\bullet}$ and $^{\bullet}OH$ are the major ROS of the nano-$CoFe_2O_4$/PMS reaction system, and in the quenching experiment, although $SO_4^{-\bullet}$ and $^{\bullet}OH$ have been quenched, the pollutants were still degraded, indicating the existence of other ROS.

To further determine the contribution of ROS in the nano-$CoFe_2O_4$/PMS reaction system, EPR measurements were carried out by using 5,5-dimethyl-1-pyrroline N-oxide (DMPO) and 4-oxo-2,2,6,6-tetramethyl piperidine (TEMP) as spin trapping agents for the determination of $SO_4^{-\bullet}$, $^{\bullet}OH$, $^{\bullet}O_2^-$ and $^1O_2$. As shown in Fig. 5b, DMPO was added to the system, and after 5 min of reaction, the signals of the DMPO-$^{\bullet}O_2^-$ and DMPO-$^{\bullet}OH$ characteristic peak with an intensity ratio of 1:1:1:1 and 1:2:2:1 appeared. Four weaker peaks appeared around DMPO-$^{\bullet}OH$, which corresponded to DMPO-$SO_4^{-\bullet}$, indicating that all of the ROS such as $SO_4^{-\bullet}$, $^{\bullet}OH$, and $^{\bullet}O_2^-$ participated in the catalyst reaction. Then, TEMP was added to another system, and the TEMP-$^1O_2$ characteristic peak with an intensity ratio of 1:1:1 appeared, indicating that $^1O_2$ was also involved in the catalytic oxidation reaction.

3.4.2. UV–Vis spectrum of the CR degradation process

The UV–Vis spectrum of the CR degradation process was sufficient to confirm that the aromatic structure of CR had been destroyed by the nano-$CoFe_2O_4$/PMS system, as shown in Fig. 6a. As a result, there are three stronger absorbent belts at the beginning of the reaction, representing two unsaturated chromogenic groups (azo) and four colour-assisting groups (amino and sulfonate sodium). Over time, the intensity of the two absorption peaks gradually decreased, indicating that CR degradation was an oxidative process and that the benzene ring structure was continuously cleaved. Therefore, these conditions illustrate that the unsaturated bond of the benzene ring is cleaved first, and then, the benzene ring forms a series of small-molecule products by ring opening and oxidation.

3.4.3. Mineralization of CR

For the degradation experiments of organic dyes, merely studying the degradation efficiency is not very convincing. During the experiment, although the target pollutant will be decomposed to obtain the effective degradation efficiency, it is very probable that new intermediate products will form [57]. Therefore, TOC detection is considered to be a necessary part of organic matter degradation experiments, and it is also an effective way to determine whether organic matter has been successfully mineralized. As shown in Fig. 6b, after 3 h of reaction, TOC removal rate reached 18.7%, and then the removal efficiency gradually decreased, and the total removal rate reached 22.3% after 6 h of reaction. This result suggests that CR is mineralized into inorganic small molecules such as CO_2 and H_2O. It can be inferred that PMS is successfully activated by nano-$CoFe_2O_4$ to generate ROS that are beneficial to the mineralization of CR. In other words, the nano-$CoFe_2O_4$/PMS system is effective for the complete removal of CR from water.

3.4.4. Possible mechanism of PMS activation by nano-$CoFe_2O_4$

Herein, according to the results of characterization analysis and ROS identification, a possible mechanism for ROS generation over the nano-$CoFe_2O_4$/PMS system was proposed, as shown in Fig. 7. The Co^{2+} and Fe^{3+} ions on the surface of the catalyst could directly interact with the inner-sphere complex of the formed HSO_5^-, which was accompanied by the valence state change of the metals, and free radicals such as $SO_4^{-\bullet}$ and $SO_5^{-\bullet}$ were produced [Eqs. (14)–(17)]. In detail, $CoOH^+$ is generated by H_2O dissociation and reacts with HSO_5^- to generate CoO^+ and $SO_4^{-\bullet}$, which can form Co^{3+} that reacts with H^+ [Eqs. (18)–(20)] [58].

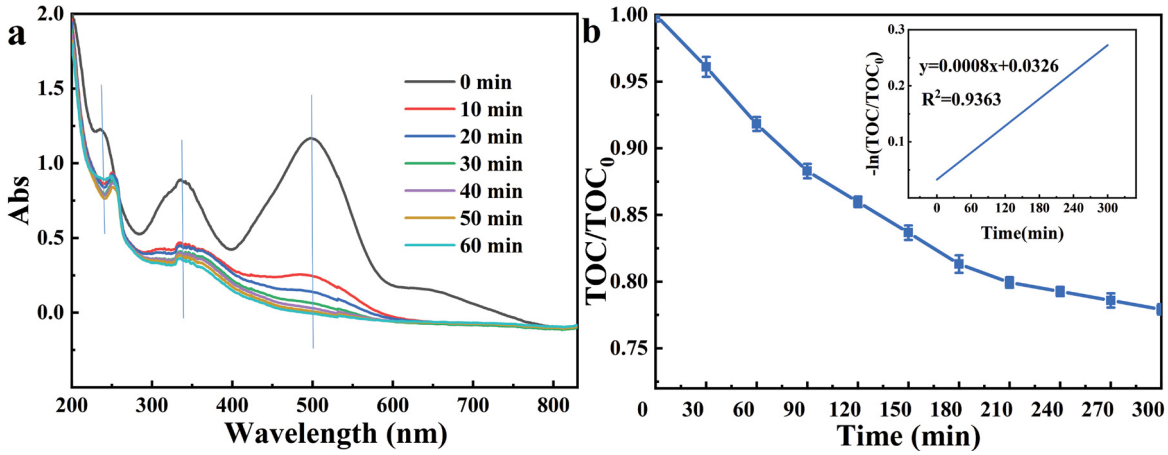

Fig. 6. Changes in UV–Vis spectra (a) and TOC (b) during CR degradation in the nano-$CoFe_2O_4$/PMS system.

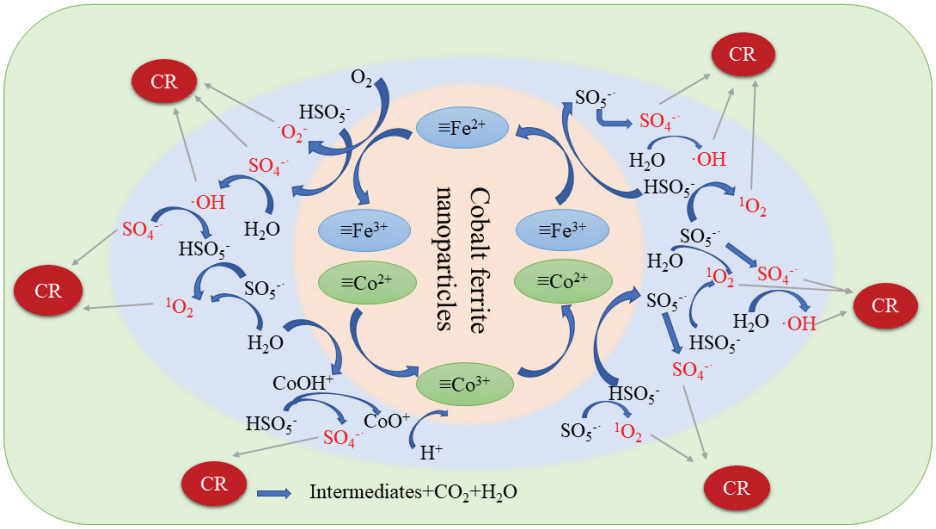

Fig. 7. Possible reaction mechanism in the nano-$CoFe_2O_4$/PMS system for CR degradation.

In addition, Co^{3+} can be reconverted to Co^{2+} by reacting with Fe^{2+} [Eq. (21)] [59]. Therefore, the metal ions on the ferrite cobalt surface form two complete cycles through the oxidation–reduction reaction for sustainable catalytic activity. Meanwhile, Fe^{2+} could also be converted to Fe^{3+} by reacting with oxygen to generate $^{\bullet}O_2^-$ [Eq. (22)]. Then, the produced $SO_4^{-\bullet}$ reacts with H_2O to generate $^{\bullet}OH$ [Eq. (23)]. HSO_5^- was formed by $SO_4^{-\bullet}$ and $^{\bullet}OH$ [Eq. (24)] and reacted with $^{\bullet}OH$ and $SO_4^{-\bullet}$ to form $SO_5^{-\bullet}$ [Eqs. (25) and (26)], respectively. In addition, the generated $SO_5^{-\bullet}$ can not only decompose to $SO_4^{-\bullet}$ [Eq. (27)] but also react with HSO_5^- and H_2O to produce $^1O_2$ [Eqs. (28) and (29)]. Ultimately, under the action of ROS such as $SO_4^{-\bullet}$, $^{\bullet}OH$, $^{\bullet}O_2^-$ and $^1O_2$, CR was degraded into some intermediate products and further mineralized into CO_2 and H_2O [Eq. (30)].

$$\equiv Co^{2+} + HSO_5^- \rightarrow \equiv Co^{3+} + SO_4^{-\bullet} + OH^- \quad (14)$$

$$\equiv Co^{3+} + HSO_5^- \rightarrow \equiv Co^{2+} + SO_5^{-\bullet} + H^+ \quad (15)$$

$$\equiv Fe^{3+} + HSO_5^- \rightarrow \equiv Fe^{2+} + SO_5^{-\bullet} + H^+ \quad (16)$$

$$\equiv Fe^{2+} + HSO_5^- \rightarrow \equiv Fe^{3+} + SO_4^{-\bullet} + OH^- \quad (17)$$

$$\equiv Co^{2+} + H_2O \rightarrow CoOH^+ + H^+ \quad (18)$$

$$CoOH^+ + HSO_5^- \rightarrow CoO^+ + SO_4^{-\bullet} + H_2O \quad (19)$$

$$CoO^+ + 2H^+ \rightarrow Co^{3+} + H_2O \quad (20)$$

$$\equiv Co^{3+} + \equiv Fe^{2+} \rightarrow \equiv Co^{2+} + \equiv Fe^{3+} \quad (21)$$

$$Fe^{2+} + O_2 \rightarrow Fe^{3+} + {}^{\bullet}O_2^- \quad (22)$$

$$SO_4^{-\bullet} + H_2O \rightarrow {}^{\bullet}OH + SO_4^{2-} + H^+ \quad (23)$$

$$SO_4^{-\bullet} + {}^{\bullet}OH \rightarrow HSO_5^- \quad (24)$$

$$HSO_5^- + SO_4^{-\bullet} \rightarrow SO_5^{-\bullet} + SO_4^{2-} + H^+ \quad (25)$$

$$HSO_5^- + {}^{\bullet}OH \rightarrow SO_5^{-\bullet} + H_2O \quad (26)$$

$$2SO_5^{-\bullet} \rightarrow SO_4^{-\bullet} + O_2 \quad (27)$$

$$SO_5^{-\bullet} + HSO_5^- \rightarrow SO_4^{2-} + HSO_4^- + {}^1O_2 \quad (28)$$

$$2SO_5^{-\bullet} + H_2O \rightarrow 2HSO_4^- + 1.5{}^1O_2 \quad (29)$$

$$CR + SO_4^{-\bullet} + {}^{\bullet}OH + {}^{\bullet}O_2^- + {}^1O_2 \rightarrow \text{intermediates} + CO_2 + H_2O \quad (30)$$

3.5. Stability and reusability of nano-$CoFe_2O_4$

The stability and reusability of nano-$CoFe_2O_4$ are important evaluation indicators related to its practical applicability. To investigate the catalytic stability of the prepared nano-$CoFe_2O_4$, five cycles of degradation experiments were carried out under the same experimental conditions. As shown in Fig. 8, the catalytic performance of nano-$CoFe_2O_4$ is relatively stable. Compared with that of the first cycle, after the second, third, fourth, and fifth cycles were performed for 60 min, the CR degradation rate decreased by approximately 0.4%, 0.7%, 2.2% and 7.2%, respectively, and the CR degradation rate remained above 83% after the fifth cycle. The reason for the decrease may be that the small-molecule intermediate products

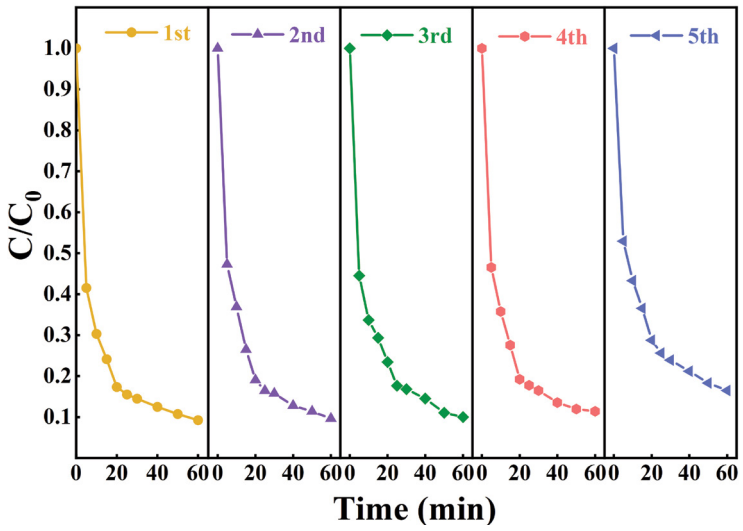

Fig. 8. Stability and reusability of nano-$CoFe_2O_4$ for CR degradation.

produced during the degradation process are attached to the surface of the catalyst so that the activity of some active sites decreases or deactivation hinders the reaction between the catalyst and PMS. In addition, the SEM, XRD, and FT-IR results confirmed that the physical and chemical properties of the catalyst scarcely changed after the reaction. In conclusion, the synthesized catalyst not only exhibited excellent efficiency in CR degradation but also revealed remarkable stability and reusability, indicating that nano-$CoFe_2O_4$ is considered to be the right choice for active PMS to degrade CR.

4. Conclusions

In this study, we obtained the following results through a comprehensive analysis of the characterization results and activation performance of nano-$CoFe_2O_4$ catalysts for CR degradation in aqueous solution:

- Based on characterization analysis results, it was proven that the nano-$CoFe_2O_4$ prepared by the co-precipitation method has the advantages of relatively high purity, small particle size and large specific surface area. Comparing the catalysts before and after the reaction, notably, the structure of the catalyst itself hardly changed. Therefore, the prepared nano-$CoFe_2O_4$ can be regarded as a catalyst with strong stability and high catalytic efficiency. Meanwhile, to solve the defect in that the catalyst easily accumulates, a more friendly method, such as biochar loading, is proposed.
- According to the identification of ROS results, it was confirmed that nano-$CoFe_2O_4$ with higher specific surface energy effectively activated PMS to release more ROS, such as $SO_4^{\bullet-}$, $^{\bullet}OH$, $^{\bullet}O_2^-$ and $^1O_2$, and important results were obtained. The catalyst can be considered a PMS activator with higher activation performance.
- In view of the CR degradation experiment results, it was further confirmed that the advanced oxidation method composed of the synthesized catalyst and PMS is undoubtedly an environmentally friendly methods that consume less time and fewer resources and has high recycling and removal efficiencies. Furthermore, the findings of this work highlighted the great potential of nano-$CoFe_2O_4$ as an activator and elucidated a new opportunity for the treatment of organic dye wastewater.

Acknowledgments

This work was supported by Natural Science Foundation of Heilongjiang Provincial of China (LH2019D002).

References

[1] C.M. Simonescu, A. Tătăruş, D.C. Culiţă, N.C. Stănică, I.A. Ionescu, B. Butoi, A.-M. Banici, Comparative study of $CoFe_2O_4$ nanoparticles and $CoFe_2O_4$-chitosan composite for Congo red and Methyl orange removal by adsorption, Nanomaterials-Basel, 11 (2021) 711, doi: 10.3390/nano11030711.
[2] R. Jiang, H.-Y. Zhu, J.-B. Li, F.-Q. Fu, J. Yao, S.-T. Jiang, G.-M. Zeng, Fabrication of novel magnetically separable BiOBr/$CoFe_2O_4$ microspheres and its application in the efficient removal of dye from aqueous phase by an environment-friendly and economical approach, Appl. Surf. Sci., 364 (2016) 604–612.
[3] D.D. Yu, H. Wang, J. Yang, Z.Q. Niu, H.T. Lu, Y. Yang, L.W. Cheng, L. Guo, Dye wastewater cleanup by graphene composite paper for tailorable supercapacitors, ACS Appl. Mater. Interfaces, 9 (2017) 21298–21306.
[4] Z.B. Duan, Y.L. Li, M. Zhang, H. Bian, Y. Wang, L.J. Zhu, D.H. Xia, Towards cleaner wastewater treatment for special removal of cationic organic dye pollutants: a case study on application of supramolecular inclusion technology with β-cyclodextrin derivatives, J. Cleaner Prod., 256 (2020) 120308, doi: 10.1016/j.jclepro.2020.120308.
[5] C.M. Teh, A.R. Mohamed, Roles of titanium dioxide and ion-doped titanium dioxide on photocatalytic degradation of organic pollutants (phenolic compounds and dyes) in aqueous solutions: a review, J. Alloys Compd., 509 (2010) 1648–1660.
[6] Y. Yoshiaki, H. Takahiro, H. Jun, Structural characteristics of xyloglucan-Congo red aggregates as observed by small angle x-ray scattering, Cellulose, 12 (2005) 469–477.
[7] M. Yu, S. Zhao, H. Wu, S Asuha, Efficient removal of Congo red by magnetically separable mesoporous TiO_2 modified with γ-Fe_2O_3, J. Porous Mater., 20 (2013) 1353–1360.

[8] F. Bessaha, N. Mahrez, K. Marouf-Khelifa, A. Çoruh, A. Khelifa, Removal of Congo red by thermally and chemically modified halloysite: equilibrium, FTIR spectroscopy, and mechanism studies, Int. J. Environ. Sci. Technol., 16 (2019) 4253–4260.
[9] S. Yavari, N.M. Mahmodi, P. Teymouri, B. Shahmoradi, A. Maleki, Cobalt ferrite nanoparticles: preparation, characterization and anionic dye removal capability, J. Taiwan Inst. Chem. Eng., 59 (2016) 320–329.
[10] K. Naseem, Z.H. Farooqi, R. Begum, A. Irfan, Removal of Congo red dye from aqueous medium by its catalytic reduction using sodium borohydride in the presence of various inorganic nanocatalysts: a review, J. Cleaner Prod., 187 (2018) 296–307.
[11] L.S. Zhang, J.S. Lian, L.X. Wang, J. Jiang, Z.R. Duan, L.J. Zhao, Markedly enhanced coercive field and Congo red adsorption capability of cobalt ferrite induced by the doping of non-magnetic metal ions, Chem. Eng. J., 241 (2014) 384–392.
[12] I. Mnif, R. Fendri, D. Ghribi, Biosorption of Congo red from aqueous solution by *Bacillus weihenstephanensis* RI12; effect of SPB1 biosurfactant addition on biodecolorization potency, Water Sci. Technol., 72 (2015) 865–874.
[13] N. El-Ahmady El-Naggar, R.A. Hamouda, M.A. Abuelmagd, S.A. Abdelgalil, Bioprocess development for biosorption of cobalt ions and Congo red from aquatic mixture using *Enteromorpha intestinalis* biomass as sustainable biosorbent, Sci. Rep., 11 (2021) S41598-021-94026-6, doi: 10.1038/s41598-021-94026-6.
[14] J. Liu, N. Wang, H.L. Zhang, J. Baeyens, Adsorption of Congo red dye on $Fe_xCo_{3-x}O_4$ nanoparticles, J. Environ. Manage., 238 (2019) 473–483.
[15] V.K. Gupta, S. Agarwal, R. Ahmad, A. Mirza, J. Mittal, Sequestration of toxic Congo red dye from aqueous solution using ecofriendly guar gum/activated carbon nanocomposite, Int. J. Biol. Macromol., 158 (2020) 1310–1318.
[16] W.-K. Jo, S. Kumar, M.A. Isaacs, A.F. Lee, S. Karthikeyan, Cobalt promoted TiO_2/GO for the photocatalytic degradation of oxytetracycline and Congo red, Appl. Catal., B, 201 (2017) 159–168.
[17] K. Indira, S. Shanmugam, A. Har, S. Vasantharaj, S. Sathiyavimal, K. Brindhadevi, A. El Askary, A. Elfasakhany, A. Pugazhendhi, Photocatalytic degradation of Congo red dye using nickel–titanium dioxide nanoflakes synthesized by *Mukia madrasapatna* leaf extract, Environ. Res., 202 (2021) 111647, doi: 10.1016/j.envres.2021.111647.
[18] O.T.H. Le, L.N. Tran, V.T. Doan, Q.V. Pham, A.V. Ngo, H.H. Nguyen, Mucilage extracted from dragon fruit peel (*Hylocereus undatus*) as flocculant for treatment of dye wastewater by coagulation and flocculation process, Int. J. Polym. Sci., 2020 (2020) 7468343, doi: 10.1155/2020/7468343.
[19] P.R. Gogate, A.B. Pandit, A review of imperative technologies for wastewater treatment II: hybrid methods, Adv. Environ. Res., 8 (2004) 553–597.
[20] P. Verma, S.K. Samanta, Microwave-enhanced advanced oxidation processes for the degradation of dyes in water, Environ. Chem. Lett., 16 (2018) 969–1007.
[21] L. Gan, Q. Zhong, A. Geng, L.J. Wang, C. Song, S.G. Han, J.Q. Cui, L.J. Xu, Cellulose derived carbon nanofiber: a promising biochar support to enhance the catalytic performance of $CoFe_2O_4$ in activating peroxymonosulfate for recycled dimethyl phthalate degradation, Sci. Total Environ., 694 (2019) 133705, doi: 10.1016/j.scitotenv.2019.133705.
[22] Q.R. Wang, Y. Shi, S. Lv, Y. Liang, P.F. Xiao, Peroxymonosulfate activation by tea residue biochar loaded with Fe_3O_4 for the degradation of tetracycline hydrochloride: performance and reaction mechanism, RSC Adv., 11 (2021) 18525–18538.
[23] L.X. Zhang, R. Zhang, W.N. Wang, S. Han, P.F. Xiao, UV-enhanced nano-nickel ferrite-activated peroxymonosulfate for the degradation of chlortetracycline hydrochloride in aqueous solution, RSC Adv., 11 (2021) 20580–20590.
[24] P.-F. Xiao, L. An, D.-D. Wu, The use of carbon materials in persulfate-based advanced oxidation process: a review, New Carbon Mater., 35 (2020) 667–683.
[25] L. An, P.F. Xiao, Zero-valent iron/activated carbon micro-electrolysis to activate peroxydisulfate for efficient degradation of chlortetracycline in aqueous solution, RSC Adv., 10 (2020) 19401–19409.
[26] Y. You, Z.K. Shi, Y.H. Li, Z.J. Zhao, B. He, X.W. Cheng, Magnetic cobalt ferrite biochar composite as peroxymonosulfate activator for removal of lomefloxacin hydrochloride, Sep. Purif. Technol., 272 (2021) 118889, doi: 10.1016/j.seppur.2021.118889.
[27] Y.-Y. Ahn, E.T. Yun, Heterogeneous metals and metal-free carbon materials for oxidative degradation through persulfate activation: a review of heterogeneous catalytic activation of persulfate related to oxidation mechanism, Korean J. Chem. Eng., 36 (2019) 1767–1779.
[28] Y.P. Bao, T.-T. Lim, R. Wang, R.D. Webster, X. Hu, Urea-assisted one-step synthesis of cobalt ferrite impregnated ceramic membrane for sulfamethoxazole degradation via peroxymonosulfate activation, Chem. Eng. J., 343 (2018) 737–747.
[29] D.X. Gao, M. Junaid, F. Lin, S. Zhang, N. Xu, Degradation of sulphachloropyridazine sodium in column reactor packed with $CoFe_2O_4$–loaded quartz sand via peroxymonosulfate activation: Insights into the amorphous phase, efficiency, and mechanism, Chem. Eng. J., 390 (2020) 124549, doi: 10.1016/j.cej.2020.124549.
[30] F.P. Hu, W.D. Luo, C.H. Liu, H.L. Dai, X. Xu, Q.Y. Yue, L. Xu, G.P. Xu, Y. Jian, X.M. Peng, Fabrication of graphitic carbon nitride functionalized P–$CoFe_2O_4$ for the removal of tetracycline under visible light: optimization, degradation pathways and mechanism evaluation, Chemosphere, 274 (2021) 129783, doi: 10.1016/j.chemosphere.2021.129783.
[31] Y. Zhao, M. Song, Q. Cao, P.Z. Sun, Y.H. Chen, F.Y. Meng, The superoxide radicals' production via persulfate activated with $CuFe_2O_4$@biochar composites to promote the redox pairs cycling for efficient degradation of *o*-nitrochlorobenzene in soil, J. Hazard. Mater., 400 (2020) 122887, doi: 10.1016/j.jhazmat.2020.122887.
[32] V.S. Kirankumar, S. Sumathi, Photocatalytic and antibacterial activity of bismuth and copper co-doped cobalt ferrite nanoparticles, J. Mater. Sci.: Mater. Electron., 29 (2018) 8738–8746.
[33] M.J. Sun, X.L. Han, S.G. Chen, Synthesis and photocatalytic activity of nano-cobalt ferrite catalyst for the photo-degradation various dyes under simulated sunlight irradiation, Mater. Sci. Semicond. Process., 91 (2019) 367–376.
[34] M. Madhukara Naik, H.S. Bhojya Naik, G. Nagaraju, M. Vinuth, K. Vinu, R. Viswanath, Green synthesis of zinc doped cobalt ferrite nanoparticles: structural, optical, photocatalytic and antibacterial studies, Nano-Struct. Nano-Objects, 19 (2019) 100322, doi: 10.1016/j.nanoso.2019.100322.
[35] X.F. Wu, W. Wang, F. Li, S. Khaimanov, N. Tsidaeva, M. Lahoubi, PEG-assisted hydrothermal synthesis of $CoFe_2O_4$ nanoparticles with enhanced selective adsorption properties for different dyes, Appl. Surf. Sci., 389 (2016) 1003–1011.
[36] S. Han, P.F. Xiao, Catalytic degradation of tetracycline using peroxymonosulfate activated by cobalt and iron co-loaded pomelo peel biochar nanocomposite: characterization, performance and reaction mechanism, Sep. Purif. Technol., 287 (2022) 120533, doi: 10.1016/j.seppur.2022.120533.
[37] R.M. Balakrishnan, I. Ilango, G. Gamana, X.-T. Bui, A. Pugazhendhi, Cobalt ferrite nanoparticles and peroxymonosulfate system for the removal of ampicillin from aqueous solution, J. Water Process Eng., 40 (2020) 101823, doi: 10.1016/j.jwpe.2020.101823.
[38] J. Mohapatra, M.Y. Xing, J. Ping Liu, Inductive thermal effect of ferrite magnetic nanoparticles, Materials, 12 (2019) 3208, doi: 10.3390/ma12193208.
[39] H. Al-aidy El-saied, E.M. El-Fawalb, Green superabsorbent nanocomposite hydrogels for high-efficiency adsorption and photo-degradation/reduction of toxic pollutants from waste water, Polym. Test., 97 (2021) 107134, doi: 10.1016/j.polymertesting.2021.107134.
[40] H.X. Zeng, W.Q. Zhang, L. Deng, J. Luo, S. Zhou, X. Liu, Y. Pei, Z. Shi, J. Crittenden, Degradation of dyes by peroxymonosulfate activated by ternary CoFeNi-layered double hydroxide: catalytic performance, mechanism and kinetic modeling, J. Colloid Interface Sci., 515 (2018) 92–100.

[41] A. Al-Anazi, W.H. Abdelraheem, C. Han, M.N. Nadagouda, L. Sygellou, M.K. Arfanis, P. Falaras, V.K. Sharma, D.D. Dionysiou, Cobalt ferrite nanoparticles with controlled composition-peroxymonosulfate mediated degradation of 2-phenylbenzimidazole-5-sulfonic acid, Appl. Catal., B, 221 (2018) 266–279.
[42] D. Oh, C.-S. Lee, Y.-G. Kang, Y.-S. Chang, Hydroxylamine-assisted peroxymonosulfate activation using cobalt ferrite for sulfamethoxazole degradation, Chem. Eng. J, 386 (2020) 123751, doi: 10.1016/j.cej.2019.123751.
[43] G.B. Jegadeesan, S. Amirthavarshini, J. Divya, G.I. Gunarani, Catalytic peroxygen activation by biosynthesized iron nanoparticles for enhanced degradation of Congo red dye, Adv. Powder Technol., 30 (2019) 2890–2899.
[44] S. Shao, L. Qian, X. Zhan, M.J. Wang, K. Lu, J.B. Peng, D. Miao, S.X. Gao, Transformation and toxicity evolution of amlodipine mediated by cobalt ferrite activated peroxymonosulfate: effect of oxidant concentration, Chem. Eng. J., 382 (2020) 123005, doi: 10.1016/j.cej.2019.123005.
[45] Z.-Y. Guan, E. Kwon, J. Lee, Y.-F. Lin, K.-Y. Andrew Lin, Electrospun cobalt ferrite nanofiber as a magnetic and effective heterogeneous catalyst for activating peroxymonosulfate to degrade sulfosalicylic acid, Sep. Purif. Technol., 259 (2021) 118163, doi: 10.1016/j.seppur.2020.118163.
[46] J.A. Mohammad, F. Alireza, A. Morteza, B.G. Nejad, M. Arshadi, Recycling bone waste and cobalt-wastewater into a highly stable and efficient activator of peroxymonosulfate for dye and HEPES degradation, Process Saf. Environ. Prot., 147 (2021) 626–641.
[47] L.J. Xu, Y.D. Wang, J. Liu, S.G Han, Z.P. Pan, L. Gan, High-efficient visible-light photocatalyst based on graphene incorporated Ag_3PO_4 nanocomposite applicable for the degradation of a wide variety of dyes, J. Photochem. Photobiol., A, 340 (2017) 70–79.
[48] H.Y. Zhou, L.D. Lai, Y.J. Wan, Y.L. He, G. Yao, B. Lai, Molybdenum disulfide (MoS_2): a versatile activator of both peroxymonosulfate and persulfate for the degradation of carbamazepine, Chem. Eng. J., 384 (2020) 123264, doi: 10.1016/j.cej.2019.123264.
[49] C.Q. Tan, N.Y. Gao, Y. Deng, Y.J. Zhang, M.H. Sui, J. Deng, S.Q. Zhou, Degradation of antipyrine by UV, UV/H_2O_2 and UV/PS, J. Hazard. Mater., 260 (2013) 1008–1016.
[50] M.C. Dodd, C.-H. Huang, Transformation of the antibacterial agent sulfamethoxazole in reactions with chlorine: kinetics, mechanisms, and pathways, Environ. Sci. Technol., 38 (2004) 5607–5615.
[51] X.H. Li, Z.H. Zhao, H.C. Li, J.S. Qian, Degradation of organic contaminants in the $CoFe_2O_4$/peroxymonosulfate process: the overlooked role of Co(II)-PMS complex, Chem. Eng. J. Adv., 8 (2021) 100143, doi: 10.1016/j.ceja.2021.100143.
[52] N. Jaafarzadeh, F. Ghanbari, M. Ahmadi, Efficient degradation of 2,4-dichlorophenoxyacetic acid by peroxymonosulfate/magnetic copper ferrite nanoparticles/ozone: a novel combination of advanced oxidation processes, Chem. Eng. J., 320 (2017) 436–447.
[53] Y. Zhao, X.Y. Ma, P.Y. Xu, H. Wang, Y.C. Liu, A. He, Elemental mercury removal from flue gas by $CoFe_2O_4$ catalyzed peroxymonosulfate, J. Hazard. Mater., 341 (2018) 228–237.
[54] J.L. Peng, H.Y. Zhou, W. Liu, Z.M. Ao, H.D. J, Y. Liu, S.J. Su, G. Yao, B Lai, Insights into heterogeneous catalytic activation of peroxymonosulfate by natural chalcopyrite: pH-dependent radical generation, degradation pathway and mechanism, Chem. Eng. J., 397 (2020) 125387, doi: 10.1016/j.cej.2020.125387.
[55] X.W. Li, X.T. Liu, C.Y. Lin, H.J. Zhang, Z. Zhou, G.X. Fan, J. Ma, Cobalt ferrite nanoparticles supported on drinking water treatment residuals: an efficient magnetic heterogeneous catalyst to activate peroxymonosulfate for the degradation of atrazine, Chem. Eng. J., 367 (2019) 208–218.
[56] Q.Y. Song, Y.P. Feng, Z. Wang, G.G. Liu, W.Y. Lv, Degradation of triphenyl phosphate (TPhP) by $CoFe_2O_4$-activated peroxymonosulfate oxidation process: kinetics, pathways, and mechanisms, Sci. Total Environ., 681 (2019) 331–338.
[57] C. Wang, J.Y. Zhao, C.M. Chen, P. Na, Catalytic activation of PS/PMS over Fe-Co bimetallic oxides for phenol oxidation under alkaline conditions, Appl. Surf. Sci., 562 (2021) 150134, doi: 10.1016/j.apsusc.2021.150134.
[58] S. Briceño, J. Suarez, G. Gonzalez, Solvothermal synthesis of cobalt ferrite hollow spheres with chitosan, Mater. Sci. Eng., C, 78 (2017) 842–846.
[59] Y.Y. Luo, C. Liu, T. Mehmood, Y.J. Zhang, M.Y. Yu, Y.Y. Ren, Activation of permonosulfate by Co-Fe_3O_4 composite catalyst for amino acid removal: performance and mechanism of Co-Fe_3O_4 nanoparticles, J. Environ. Chem. Eng., 9 (2021) 106036.